Supporting Information:

Strong Coupling in a Self-Coupled Terahertz Photonic Crystal

Maria Kaeek, Ran Damari, Michal Roth, Sharly Fleischer and Tal Schwartz

Physical Chemistry Department, Raymond and Beverly Sackler Faculty of Exact Sciences and Tel Aviv Center for Light-Matter Interaction, Tel Aviv University, Tel Aviv 6997801, Israel.

S1. SAMPLE PREPARATION

The α-lactose samples were prepared by pressing α-lactose powder into a pellet, using a pressing die (19 mm diameter) at a pressure of 220 kN for 10 minutes. In order to perform consecutive measurements of the grating and the reference while keeping the same conditions, we designed and fabricated a micro-machined pressing die, where half of the surface was kept smooth while the other half had a periodic array of triangular grooves. Pressing the α-lactose powder using this plate yielded a pellet having the complementary shape on its surface and composed of two adjacent sections - one smooth, to be used as the reference and the other having a periodic array of triangular ridges forming the 1D photonic crystal. In this way, the reference and the photonic crystal have an identical thickness t. Moreover, by mounting the sample on a motorized linear translation stage, we could alternate between the grating and the reference without replacing the sample and without opening the purged measurement chamber.

The thickness of the grating substrate (t) was controlled by adjusting the amount of lactose powder used in pressing the pellet. To obtain a thickness of 90±6 μm we used 40 mg of α-lactose powder while 90 mg yielded a 245±6 μm pellet.

S2. THZ TIME-DOMAIN SPECTROSCOPY

The measurements were performed using a home-built time-domain terahertz spectroscopy setup, as used in our previous study.[S1] In essence, the single-cycle THz pulse was generated using titled pulse-front optical rectification in a $LiNbO_3$ crystal, and the THz field measurement was performed by time-resolved electro-optic sampling in a GaP crystal. The setup was placed in a closed chamber and purged with dry air to keep a low relative humidity of 7% to prevent THz absorption by water vapor. Time-domain signals were acquired over a range of 90 ps (starting at -33 ps relative to the incoming THz pulse) at a constant time step of 133 fs and averaged over ten and two

scans for the thin and thick samples, respectively, to reduce the effect of slow laser intensity variations. At each step the signal was averaged over 50 laser pulses to reduce the effect of measurement noise.

As a result of optical reflections at the interfaces of the electro-optic crystal, the time-resolved electro-optic sampling technique typically gives rise to several artificial satellite signals at both negative and positive times, in particular when measurements are performed over a long range of time (~10-100 ps), as illustrated in Figure S1. In order to remove these spurious signals from the measured signals $S_M(t)$, we first obtained the instrument response function using $\hat{H}(f) = \hat{A}(f)/\hat{P}(f)$, where $\hat{A}(f)$ is the Fourier transform of the time-resolved measurement of the THz pulse going through air (denoted as $A(t)$ in Figure S1) and $\hat{P}(f) = \mathcal{F}\{P(t)\}$ is the Fourier transform of the isolated single-cycle pulse. This, in turn, is obtained by keeping $A(t)$ only at the interval $-5\ \text{ps} < t < 5\ \text{ps}$ and zero-padding the rest of the time domain. Then, we deconvolved the instrument response function from the measured signals to obtain the real signal $S(t)$ using $S(t) = \mathcal{F}^{-1}\{\hat{S}_M/\hat{H}\}$, with $\hat{S}_M(f) = \mathcal{F}\{S_M(t)\}$.

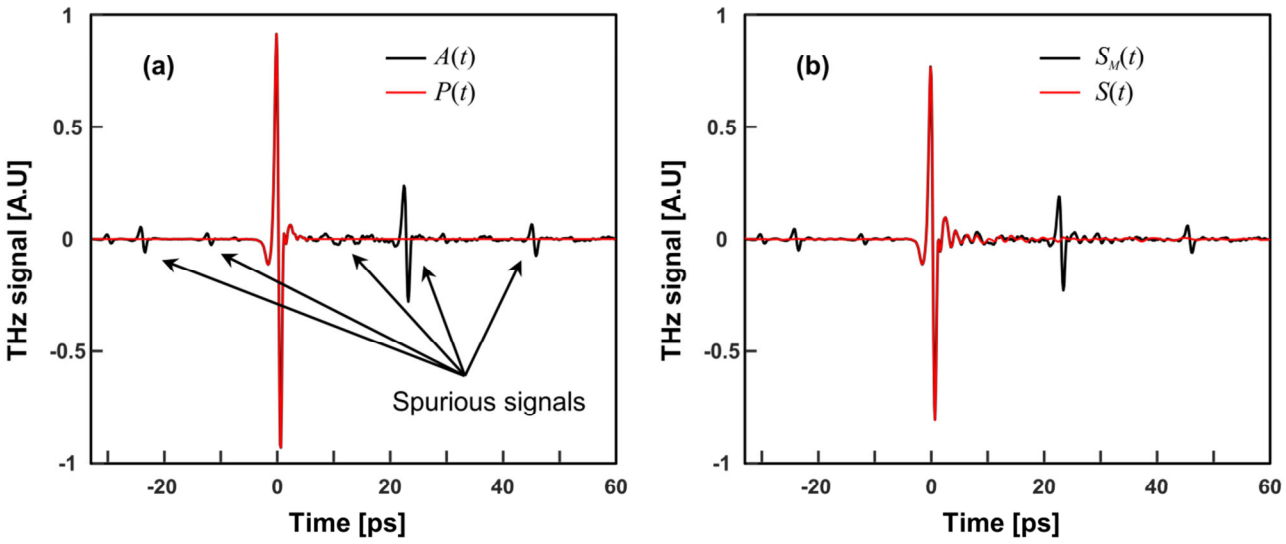

Figure S1. (a) Data used for obtaining the instrument response function. The black curve shows the as-measured THz field for a single-cycle pulse propagating through air and the red curve is the real time-domain signal representing the isolated original pulse. (b) The as-measured signal for the α-lactose photonic crystal (black curve) and the deconvolved signal with the spurious reflections removed (red curve).

S3. NUMERICAL SIMULATIONS

In order to simulate the spectral response of the sample and to obtain the angle-resolved transmission spectra we used the Rigorous Coupled-Wave Analysis (RCWA) method,[S2,S3] which is commonly used for simulating the spectral radiative properties of layered optical structures with in-plane periodic modulation. In essence, RCWA is a Fourier-plane method in which the Floquet modes for each layer are calculated and then matched at the boundaries between the various layers. We used a publicly available Matlab code developed by the Zhang group at Georgia Tech (available at http://zhang-nano.gatech.edu/).

In our simulations, we mimic the periodic layer by considering rectangular ridges having a width and height of 50 μm, chosen such that the overall area is equal to the area of the triangular ridges in the samples used for the experiments. For the frequency-dependent dielectric function of α-lactose we used a Lorentz-Drude model with contributions from three different vibrational transitions:

$$\varepsilon_{\alpha L}(f) = \varepsilon_0 \left[\varepsilon_\infty + \sum_{i=1}^{3} \frac{f_{p,i}^2}{f_i^2 - f^2 - i\gamma_i f} \right] \qquad \text{(S1)}$$

where ε_0 is the vacuum permittivity, $\varepsilon_\infty = 3.2$ is the (relative) background dielectric constant , f_i = 0.53, 1.195, and 1.37 THz are the vibrational frequencies, γ_i = 21, 44, and 58 GHz are the linewidths, and $f_{p,i}$= 0.123, 0.072, and 0.253 THz are the corresponding plasma frequencies.[S4]

Apart from providing the transmission spectra for the periodic structure, the RCWA simulations can also be used for obtaining the spatial field distribution within the structure for an incoming plane wave at a given angle. In order to find the modal field distribution presented in the insets of Figure 4 and Figure 5, we used the following procedure: First, the field distribution $E_0(x, z)$ for a homogeneous slab (of thickness t) without the ridge layer was calculated for a plane wave with given in-plane momentum and frequency. Then, the simulations were repeated for the full 1D photonic crystal under identical incoming planewave but with the ridge added on top of the homogeneous slab. Using these results, we then calculated the modal field as $E_{mode} = Re\{E_{PC} - E_0\}$, where $E_{PC}(x, z)$ is the field distribution for the photonic crystal.

S4. CALCULATION OF THEORETICAL DISPERSION CURVES

Neglecting the ridge array, the free-standing lactose sample can be considered as a symmetric slab waveguide with a thickness t and air cladding. The frequencies of the uncoupled bound states of the waveguide as a function

of their in-plane momentum (propagation constant) k_{wg} can be found by seeking the multiple (real) poles of the reflection/transmission through the dielectric layers, $f^{(n)}(k_{wg})$, which obey the characteristic eigenvalue equation[S5]

$$1 - r_{TE/TM}^2 e^{ik_{z,1}t} = 0 \qquad \text{(S2)}$$

with $r_{TE} = \frac{k_{z0}-k_{z1}}{k_{z0}+k_{z1}}$ and $r_{TM} = \frac{k_{z0}-k_{z1}/\varepsilon_\infty}{k_{z0}+k_{z1}/\varepsilon_\infty}$ being the reflection amplitudes for TE and TM polarization, respectively and $\mathrm{k_{z0}} = \sqrt{k_0^2 - k_{wg}^2}$ and $\mathrm{k_{z1}} = \sqrt{\varepsilon_\infty k_0^2 - k_{wg}^2}$ are the out-of-plane components of the wave-vectors in air and in the dielectric layer, with $k_0 = \frac{2\pi f}{c}$. For such bound states one requires that $\mathrm{k_{z0}}$ is imaginary, signifying evanescent decay into air, which occurs when $k_{wg} > k_0$ (i.e., beyond the air light line).

In order to calculate the dispersion of the vibration-coupled modes (dashed blue curves in Figure 1c), we replace ε_∞ with the full (relative) complex dielectric function of α-lactose $\varepsilon_{\alpha L}(f)/\varepsilon_0$, as given by equation S1. In this case, the eigenfrequencies become complex (for real values of k_{wg}), with the imaginary part signifying the finite lifetime (and linewidth) of the polaritonic modes due to absorption in the material.[S6] Note that Figure 1c presents the real part of $f(k_{wg})$ for the polaritonic dispersion.

With the addition of the periodic ridge array (and neglecting the slight change in the effective width of the waveguide due to the added material) the various dispersion branches of the 1D photonic crystal can be simply calculated by inverting the dispersion relation for the various waveguide modes to obtain $k_{wg}^{(n)}(f)$ and then adding/subtracting a reciprocal lattice vector such that

$$k_x^{(n,m)} = k_{wg}^{(n)}(f) + \frac{2\pi}{P} m \qquad \text{(S3)}$$

where $m = 0, \pm 1, \pm 2$ ... is the diffraction order and P is array periodicity.

S5. FABRY-PÉROT EFFECT IN REFERENCE FILM

As shown in Figure 3a, the transmission spectra of the smooth reference film exhibit weak modulation due to the mild reflections at the two lactose-air interfaces. This can be understood by recalling the Fabry-Pérot expression for the transmitted intensity, which, for a symmetric structure and transparent dielectric slab (i.e. away from the absorption peak), takes the form[S7]

$$T(f) = \left\{1 + \left(\frac{2F}{\pi} sin\frac{\delta}{2}\right)^2\right\}^{-1} \quad \text{(S4)}$$

with $F = \frac{\pi\sqrt{R}}{1-R}$ being the finesse (where R is the intensity reflectivity of the interfaces) and $\delta = (4\pi n_{\alpha L} tf/c)cos\ \theta_M$ is the round-trip phase, where $n_{\alpha L} = \sqrt{\epsilon_\infty} = 1.78$ is the background refractive index of the α-lactose and θ_M is the propagation angle within the medium. Using the Fresnel equations we obtain that, for incident angles of $0 - 45°$, the finesse is rather low (in the range of ~1-1.5), which explains the low modulation depth of the Fabry-Pérot effect (with minimal transmission of $\{1 + (2F/\pi)^2\}^{-1} \simeq 0.5$). With the peak position (i.e. $T = 1$ or $\delta = 2\pi l$, with l being an integer number and signifying constructive interference between the multiple reflections) given by $f_{max} = \frac{cl}{2n_0 t cos\theta_M}$ and using Snell's law, one expect to observe a spectral shift of ~9% when the angle of incidence is varied from 0° to 45° (and $0 < \theta_M < 23°$), as observed in our measurements (Figure 3a) as also in the simulation results below (Figure S2).

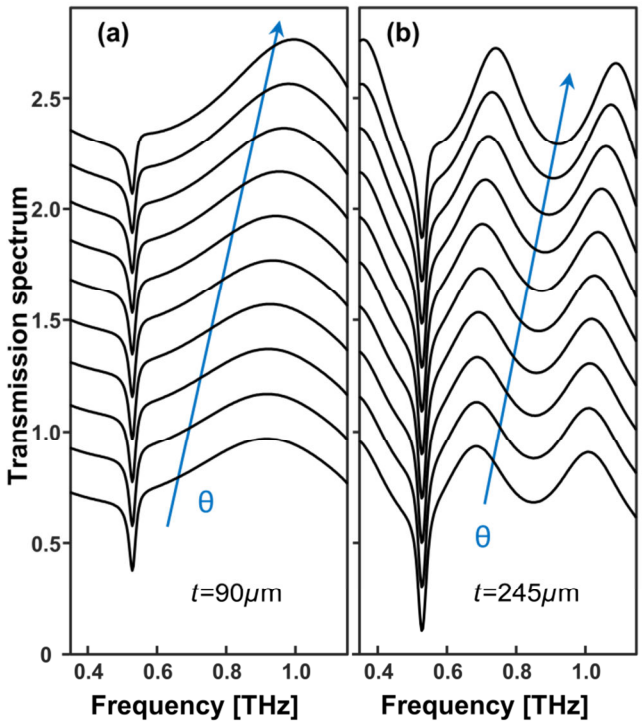

Figure S2. Simulated transmission spectra of the smooth references films with t = 90 μm (a) and t = 245 μm at incident angle of θ = 0,5, … 45°, illustrating the angle dependence of the Fabry-Pérot effect. The spectra were calculated using the T-matrix method, with the full frequency-dependent dielectric function of α-lactose (equation S1).

S6. COUPLED OSCILLATOR MODEL

In order to extract the coupling strength from the experimental dispersion diagrams, we fitted the polaritonic branches seen in Figure 4a and Figure 5a to the theoretical polariton dispersion obtained from the coupled-oscillator model, which is given by

$$f^{\pm} = \frac{f_{\mathrm{PC}}+f_{\mathrm{vib}}}{2} \pm \frac{1}{2}\sqrt{{f_R}^2 + (f_{\mathrm{PC}} - f_{\mathrm{vib}})^2} \qquad \text{(S5)}$$

where f_{PC} is the frequency of the bare photonic crystal mode interacting with the vibrational transition (obtained using equations S2-S4 and depicted by the solid lines in Figures 4a and 5a), $f_{\mathrm{vib}} = 0.53$ THz is the vibrational frequency and f_R is the Rabi frequency. The results of the fit for the two different thicknesses are presented in Figure S3, overlaid on top of the measured dispersion map. For $t = 90\ \mu m$ (Figure S3a) we used the $(n = 1, m = -1)$ branch for the bare photonic mode frequency $f_{\mathrm{PC}}(k_x)$, whereas the $(n = 2, m = -1)$ branch was used when fitting the results for $t = 245\ \mu m$ (Figure S3b).

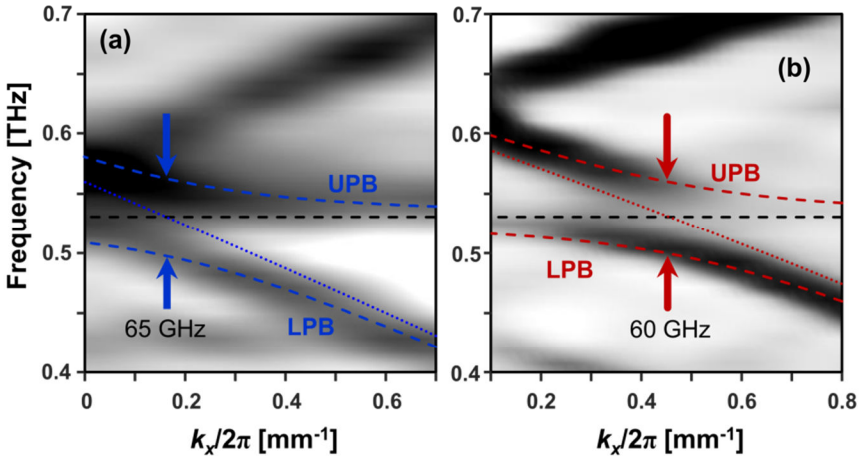

Figure S3. Theoretical dispersion curves for the lower (LPB) and upper (UPB) polariton branches, obtained from the coupled-oscillator model and fitted to the experimental results with (a) t = 90 μm (dashed blue lines) and (b) $t = 245\ \mu m$ (dashed red lines). The horizontal black lines mark the position of the vibrational frequency f_{vib} and the dotted lines are the bare photonic mode dispersion curves $f_{\mathrm{PC}}(k_x)$ used for fitting equation S6 to the experimental results, which are depicted by the gray-scale images (displaying the same data as in Figures 4a and 5a, over a smaller region).

S7. POLARIZATION DEPENDENCE OF DISPERSION MAPS

The 1D photonics crystal sets an inherent asymmetry in the structure, leading to differences in the dispersion between TE polarization (electric field parallel to the ridges) and TM polarization (electric field perpendicular to the ridges). However, since the solutions to the waveguide modes (equations S2-S3) can be found for both polarizations, the resonances of the photonic crystal also exist for both polarization, however, with quantitatively different dispersion diagrams. These differences can be seen in Figure S4, which presents the results of the RCWA simulations for the two samples.

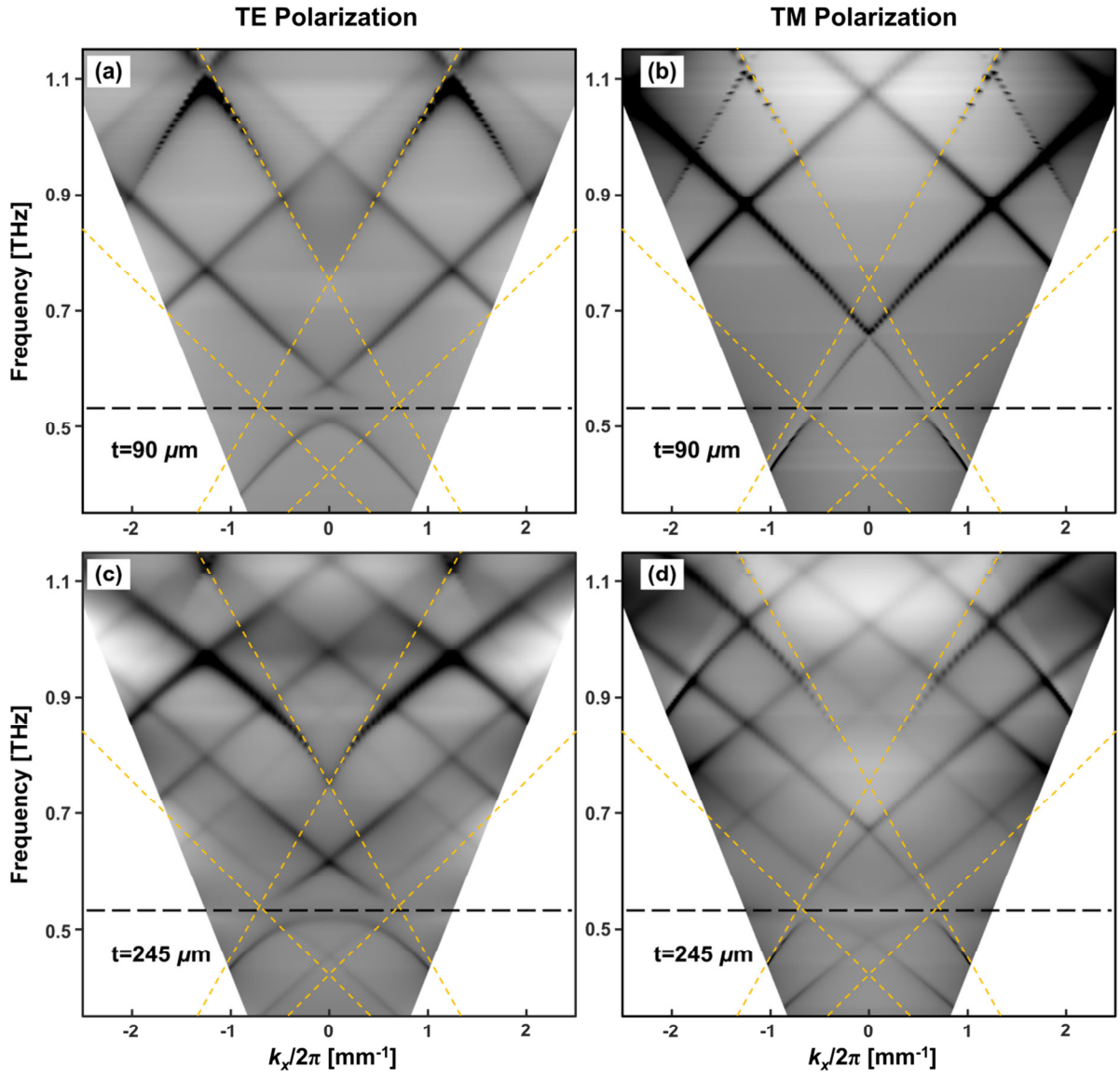

Figure S4. Dispersion diagrams obtained by RCWA simulations for the lactose photonic crystals used in the experiments, comparing TE polarization (a,c) and TM polarization (b,d). The simulations were performed with $t = 90$ µm (a,b) and $t = 245$ µm (c,d). The dashed yellow lines mark the light lines of air and lactose, shifted by one reciprocal lattice vector.

REFERENCES

(S1) Damari, R.; Weinberg, O.; Krotkov, D.; Demina, N.; Akulov, K.; Golombek, A.; Schwartz, T.; Fleischer, S. Strong coupling of collective intermolecular vibrations in organic materials at terahertz frequencies. *Nat. Commun.* **2019**, *10*, 3248.

(S2) Moharam, M. G.; Gaylord, T. K.; Grann, E. B.; Pommet, D. A. Formulation for stable and efficient implementation of the rigorous coupled-wave analysis of binary gratings. *J. Opt. Soc. Am. A* **1995**, *12*, 1068.

(S3) Zhao, B.; Zhang, Z. M. Study of magnetic polaritons in deep gratings for thermal emission control. *J. Quant. Spectrosc. Radiat. Transfer.* **2014**, *135*, 81–89.

(S4) Roggenbuck, A.; Schmitz, H.; Deninger, A.; Mayorga, I. C.; Hemberger, J.; Güsten, R.; Grüninger, M. Coherent broadband continuous-wave terahertz spectroscopy on solid-state samples. *New J. Phys.* **2010**, *12*, 043017.

(S5) Marcuse, D. *Theory of Dielectric Optical Waveguides*; Elsevier, 1991.

(S6) Canales, A.; Baranov, D. G.; Antosiewicz, T. J.; Shegai, T. Abundance of cavity-free polaritonic states in resonant materials and nanostructures. *J. Chem. Phys.* **2021**, *154*, 024701.

(S7) Yariv, A.; Yeh, P. *Photonics: optical electronics in modern communications*; Oxford University Press: New York, 2007.